Impacts of Phase-Locked Loop and Reactive Power Control on Inertia Provision by DFIG Wind Turbine

Li Sun, *Student Member, IEEE,* Xiaowei Zhao

***Abstract*—This paper evaluates the impacts of the phase-locked loop (PLL) and reactive power control (RPC) on the inertia provision of DFIG wind turbine (WT), by taking a wide range of system loading conditions (i.e., from the reactive injection to absorption) into consideration. First, a linearized model is developed for DFIG WT to describe the motion of its internal voltage phase, and the derived motion equation provides a way for analytical estimation on DFIG WT's inertia provision. After formulating the equivalent inertia, it is then used to conduct a character study on the equivalent inertia subject to different PLL and RPC settings. In this course, the loading condition of DFIG WT changes from the reactive injection to absorption to give a systematic study. Finally, the theoretical outcomes are validated by the simulations on a modified 3-machine, 9-node test system.**

***Index Terms*—DFIG wind turbine, inertia character, loading condition, phase-locked loop, reactive power control.**

NOMENCLATURE

$L_s,\ L_m$	Stator and mutual inductance
$x_s,\ x_m$	Stator and mutual inductive impedance
$\omega_1,\ \omega_b$	Unit/base value of synchronous speed
$\omega_p,\ \theta_p$	PLL angular frequency and output angle
$\theta_r, \omega_r,\ \omega_{slip}$	Rotor angle, rotor angular speed, slip speed
$P_m,\ H$	Mechanical power and equivalent mechanical inertia
$P,\ Q$	Electrical active and reactive power
$T_e^{ref},\ T_a$	Electrical torque reference
$T_{e\omega}$	Torque command from rotor speed control
T_a	Torque correction from additional inertia control
$\boldsymbol{E},\ \boldsymbol{V}$	Internal voltage and terminal voltage vectors
$\boldsymbol{I},\ \boldsymbol{\psi}$	Current and flux vectors
$E,\ V,\ I$	Magnitude of $\boldsymbol{E},\ \boldsymbol{V},\ \boldsymbol{I}$
$\boldsymbol{E_p},\ E_p$	Fictitious internal voltage vector and its magnitude
$k_{p\omega},\ k_{i\omega}$	PI parameters of rotor speed control
$k_{pp},\ k_{ip}$	PI parameters of PLL
$k_{iq},\ k_{iv}$	Parameters of reactive power control
Δ	Perturbational component of variables
MPPT	Maximum power point tracking

Superscripts and subscripts:

$ref,\ 0$	Reference, steady-state value
$s,\ r,\ g$	Stator, rotor-side, grid-side variables
$d,\ q$	d-axis, q-axis variables
p	PLL reference frame

I. INTRODUCTION

WITH the increasing integration of wind generation into power systems, the power systems are becoming weaker with decreasing inertia [1]–[3]. The lack of inertia may lead to a limit on the admissible penetration level of wind generation (i.e., "hosting capacity" [2]), as well as sharp and large frequency excursions. The risk of a system collapse increases as a result. Beyond this, the voltage is no longer stiff enough against an event of power deficiency or surplus. To sustain the stable operation of low-inertia and weak systems, wind generation has been invoked to provisionally stabilize the system frequency and voltage through control modifications. Considered as imperative, the performance requirements and auxiliary services of wind generation connected to less-inertia power systems have been defined, which are usually described in the form of a grid code [3], [4]. In addition, some top-notch working groups from a number of international utilities, manufacturers and consultants have complied a significant quantity of experiences associated with the auxiliary services of wind generation. These working groups include the IEEE 1547 working group [1], National Renewable Energy Laboratory (NREL) [5] and CIGRE [6].

The frequency control is typically embedded in the active power control (APC) of wind generation (take the mainstay-DFIG wind turbine (WT)- as an example) [7]–[9]. Inertia estimation studies of wind generation having frequency control is very critical since the inertia and frequency support is not constant anymore [10]–[12]. A mathematical formulation of the emulated inertia was established in [11]–[13]. Authors concluded that the inertia character exhibited by wind generation is mainly sensitive to APC (include the frequency control) at a given loading condition. In addition, the inertia is always cast to be effective/positive, to limit the speed of frequency dropping/rising during a low/high-frequency event, thereby stabilizing short-term frequency transients [10].

While the voltage support control is being of need in a weak system, the DFIG WT is required to provide a considerable range of reactive power capability (from the reactive -injection to -absorption (like with a ± 0.5 p.u. area)), along with a strict adherence to the requirements on var compensation/voltage-regulation capability [3], [5], [14]. In this sense, it becomes nontrivial to consider the coupled impacts of reactive power control (RPC) on the inertia character. The reference [15] proposes an idea for the inertia provision through reactive power channel. However, the reactive absorption of DFIG WT during the system frequency events tends to degrade the inertia provision, but this is not involved in this work.

The papers cited above have declared that RPC, phase-locked loop (PLL) and loading conditions play an important role in determining the active power modulation behavior and thus the inertia character [10]–[15]. However, a clear understanding about the impacts of PLL and RPC on the inertia provision by DFIG WT is still in stark, and in addition, some undesired phenomena (like the negative inertia in Section

This work was funded by the UK Engineering and Physical Sciences Research Council under grant EP/S001905/1.

L. Sun and X. Zhao (corresponding author) are with the Intelligent Control & Smart Energy (ICSE) Research Group, School of Engineering, University of Warwick, Coventry, CV4 7AL, U.K. (e-mail: Li.Sun.1@warwick.ac.uk; xiaowei.zhao@warwick.ac.uk).

IV)) that possibly appear against uncertain system loading conditions are still not discovered or estimated. Notably, the occurrence of a negative inertia must be avoided, since it provokes DFIG WT to create an under/over-production power during a low/high-frequency event and hence the power imbalance phenomenon would be deteriorated, leading to a sharp frequency drop/rise (or even a frequency collapse) in power systems.

To provide a systematic explanation on the impacts of PLL and RPC, this paper aims to investigate the inertia character of DFIG WT under possible PLL and RPC settings and system loading conditions, in a mathematical and analytical way. We first define the synthetic internal voltage of DFIG WT to present its output power dynamic properties, and henceforth establish the motion equation to characterize the electromechanical dynamic of the internal voltage phase. On this basis and considering a wide range of operating conditions, the contribution toward evaluating the impacts of PLL and RPC on inertia provision by DFIG WT, are highlighted as follows.

- To quantitatively describe the factors that impact the inertia provision, we define the synthetic internal voltage of DFIG WT to present its output power dynamic properties, and henceforth establish the motion equation to characterize the electromechanical dynamic of the internal voltage phase.
- The control blocks of the active and reactive power loop associated with the electromechanical dynamics are considered in the modelling which is then used to formulate the inertia of DFIG WT. Note that the proposed model is built for the electromechanical dynamic analysis of DFIG WT. (i) It provides a new dimension to understand the coupling between active and reactive power by converting the RPC-related factors to the APC loop; and (ii) while the proposed model separately describes the inertia and damping components, the reactive loading level is considered as a factor in the inertia formulation.
- Through varying control settings or system loading conditions, the impacts of PLL and RPC on the inertia provision are graphically described and analytically examined by measuring the inertia.

We mention that the proposed model in this paper differs from the model developed in [16] (which is for DC-link voltage stability analysis) and that unlike the model in [11], [13], the proposed model includes the RPC and its coupling with APC. The analysis results provide a guidance for manufacturers to reshape/improve and for the operators to supervise/correct the inertia provision by DFIG WT, thus help eliminate a threat of negative-inertia phenomena.

The remainder of this paper is structured as follows. Section II introduces the basic control and problem set related to the inertia provision by DFIG WT. In Section III, a linearized DFIG WT model is developed which describes the motion of synthetic internal voltage phase. According to this model, the equivalent inertia is formulated; the parameters of PLL and RPC, and the coefficients depending on the system loading condition appear in the inertia formulation. Section IV conducts a character study on the equivalent inertia under different PLL and RPC settings. These analysis results are validated in Section V. The paper is finally brought to conclusions in Section VI.

II. Problem Setup of Inertia Provision by DFIG WT

A. Review on APC and RPC of DFIG WT

The DFIG WT typically adopts a stator voltage-oriented and decoupled dual-loop control in rotor-side converter (RSC), as given in Fig. 1. The outer control regulates either the rotor speed or active power, and the inner control regulates the rotor current. Since the lower-level control is significantly faster than the electromechanical dynamic of interest in this study, the bias of the real current with respect to its reference can be omitted (i.e., $i_{rd} = i_{rd}^{ref}$ and $i_{rq} = i_{rq}^{ref}$). In addition, the slow-action pitch angle control would be not included hereafter [11].

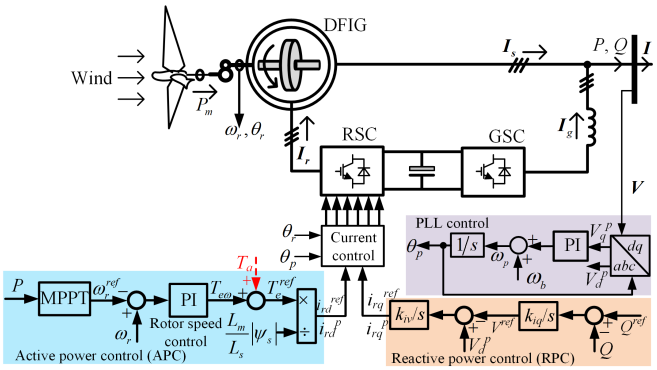

Figure 1. The block diagram of DFIG WTs with stator voltage orientation.

In Fig. 1, the generated frequency by PLL synchronization control-based DFIG WT is synthesized by two portions, i.e., (i) the DFIG and its decoupled power control ($P-Q$ control), and (ii) the stator PLL [17]. They provide two ways to design inertia emulation control. The first way is referred to df/dt inertia control [18] that is commonly used to produce a positive electrical/power correction command (superposed on the original $P-Q$ control). However, df/dt inertia control may be criticized due to the use of a pure derivative df/dt, which amplifies the adverse effect of the noise in the frequency measurement [10]. When using a high-pass filter to emulate the derivative action, it adds an extra tuning parameter (with increasing the control complexity), and introduces lags in the response of df/dt inertia control [19]. The second way is PLL tuning [11] that tries to make the phase placement (i.e., the integral of the generated frequency) more rigid, thereby creating a relatively large power angle and over-production power delivery during low-frequency events. PLL tuning is favored for implementation since it prevents reliance on any external signal and control modification.

It is of interest to note that the inertia provision through PLL tuning is no longer constant due to the dynamic complexity of DFIG WTs' control system. This has been proved in [11]. When a slow-action PLL that has a similar time frame to the power control is used for inertia emulation, the inertia provision by DFIG WTs is hard to be clamped at a given value

due to an elastic coupling between the power control and PLL. The property of such a non-constant inertia is similar to that of the equivalent inertia of a multi-mass SG, when it is modeled as a transfer function so that the elastic interaction can be exhibited [11]. Differing from the SG, the non-constant inertia of DFIG WTs is allowed to be shaped and programmed thanks to the controllability and flexibility. The reference [11] declares that setting different PLL parameters enables to achieve the desired inertia provision and also the damping requirement. In the literature, there are many other inertia emulation methods, including the prevalent df/dt inertia control [19] and virtual synchronous control [13]. Although these inertia methods have different control implementations, they all enable WTs to offer a non-constant inertia instantaneously and spontaneously. In this sense, the manufactures like General Electric (GE) have claimed that the synthetic inertia of wind generation needs to focus on functional behavior and grid response: *do not try to exactly replicate synchronous machine behavior* [20]; the grid code requirement on the inertia provision of wind generation is usually no longer limited to a precise or constant value [4], [21].

B. Problem setup

The rotor speed control is also APC owing to the use of a one-to-one correspondence between them. Thus, the active channel mainly consists of DFIG, speed control and PLL (see Fig. 1), whilst the reactive channel is represented by RPC. The behaviors of such two channels in DFIG WT are decoupled in steady-state analyses [22]. This manipulation is based on two factors: (i) owing to the stator-voltage orientation, the active power delivered from DFIG WT can be independently controlled by the d-axis rotor current, while the delivered reactive power can be controlled by the q-axis rotor current [22], [23]; and (ii) for a system with a low resistance-inductance ratio (typically, $R/X < 0.1$), the active and reactive power transfers separately adhere to the power angle and terminal voltage magnitude [24].

By considering a wide range of the system loading conditions, the inertia provision by DFIG WT would be dependent on the dynamics of both the APC and the RPC channels. The PLL behavior and the interaction of RPC with APC would be the upmost concern in this context. As the previous discussed, PLL has a contribution in the inertia provision and the amount of the inertia provision is significantly related to the PLL behavior. On the other hand, the voltage excursion actually exists at all nodes accounting for a frequency event caused by an increment of the load power in power systems. It has a relatively large value in a weak system and a prolonged transient for a slow-action RPC. The consequence of a considerable voltage excursion is a constrain on the inertia provision and/or the over-production power delivery from DFIG WT. In addition, it is to be found that the inertia provided by DFIG WT would be positive or negative depending on the reactive loading condition (see Section IV). The consequence of the negative inertia is an under-production power fed from WT during the low-frequency event, thereby exaggerating the frequency drop speed and threatening the frequency stability. However, the factors of RPC settings and loading conditions are still rarely involved in the character study on the inertia provision of DFIG WT. A further investigation and explanation on this would be carried out in this context.

III. Linearized DFIG WT model

In this section, a linearized DFIG WT model is developed seen from the motion of the synthetic internal voltage, in order to facilitate the following analysis. Next, we conduct an analytically estimation on the equivalent inertia. It gives that the PLL and RPC parameters and the coefficients related to system loading condition are all included in the formulation of the equivalent inertia.

A. Equivalent Circuit of DFIG WTs

1) Internal voltage of DFIG WTs: For DFIG WTs, the decoupling of APC and RPC is realized by the stator voltage orientation and PLL (see Fig. 1). The stator voltage $\boldsymbol{V}$ and stator flux $\boldsymbol{\psi}_s$ equations of DFIG can be derived in complex vector form and with the generator convention

$$\boldsymbol{V} = -R_s\boldsymbol{I}_s + d\boldsymbol{\psi}_s/dt + j\omega_1\boldsymbol{\psi}_s, \tag{1}$$

$$\boldsymbol{\psi}_s = -L_s\boldsymbol{I}_s + L_m\boldsymbol{I}_r \tag{2}$$

Substituting (2) for $\boldsymbol{\psi}_s$, (1) becomes

$$\boldsymbol{V} = -(R_s\boldsymbol{I}_s + jx_s\boldsymbol{I}_s + \frac{dL_s\boldsymbol{I}_s}{dt}) + (\frac{dL_m\boldsymbol{I}_r}{dt} + jx_m\boldsymbol{I}_r) \tag{3}$$

where $x_s = \omega_1 L_s$ and $x_m = \omega_1 L_m$. Discarding R_s and current transients [23], (3) is rearranged as

$$\boldsymbol{V} = -jx_s\boldsymbol{I}_s + jx_m\boldsymbol{I}_r \tag{4}$$

According to (4), we can define the internal voltage vector $\boldsymbol{E}$ of DFIG WT as

$$\boldsymbol{E} = jx_m\boldsymbol{I}_r \tag{5}$$

and the expressions of $\boldsymbol{E}$ in the dq-frame are

$$E_q = x_m i_{rd},\ E_d = -x_m i_{rq} \tag{6}$$

In addition, $\boldsymbol{E}$ has a phase as given by

$$\theta_E = \arctan(E_q/E_d) \tag{7}$$

Therefore, the concept of internal voltage is well generalized to characterize DFIG WTs' behaviors.

2) Power-transmission equations: Notably, the power fed from a DFIG WT also derives from grid-side converter (GSC), precisely equalling to the rotor power when neglecting the loss. Consider that the active power (P_g) delivered by GSC is approximately equal to the slip of stator output power (P_s) and that the output reactive power (Q_g) of GSC is generally controlled to be zero. We get

$$P_g = -\omega_{slip}P_s = -\omega_{slip}(V_d i_{sd} + V_q i_{sq}), Q_g = 0 \tag{8}$$

In the terminal voltage frame, $V_d \approx 1$ pu and $V_q = 0$. Then, the total current fed into the grid is

$$\begin{aligned} i_d &= i_{sd} + P_g/V_d = (1-\omega_{slip})i_{sd} \\ i_q &= i_{sq} - Q_g/V_d = i_{sq} \end{aligned} \tag{9}$$

By manipulating (4) in the dq-frame, we obtain

$$V_d = x_s i_q + E_d, V_q = -x_s i_d/(1-\omega_{slip}) + E_q \tag{10}$$

In addition, the active and reactive power totally fed from a DFIG WT can be written as

$$P = V_d i_d + V_q i_q, Q = -V_d i_q + V_q i_d \tag{11}$$

According to (10), a DFIG WT can be treated as a synchronous generator (SG) whose equivalent reactance is asymmetrical and associated with rotor slip. Importantly, the advantage of DFIG WT is that its internal voltage is directly determined by RSC control and thus highly controllable.

It is noteworthy that the equations (1)-(11) correspond to the terminal voltage frame, whose d-axis coincides with the terminal voltage direction. However, the converter control is realized through PLL synchronization control. PLL usually tracks the terminal voltage with its output θ_p (see Fig. 1)

$$\theta_p = ((k_{pp} + k_{ip}/s)V_q^p + \omega_b)(1/s) \tag{12}$$

and $\theta_{p0} = 0$ in the steady state. The conversion matrices amongst these two frames are given in Appendix. A.

B. Linearized Model of DFIG WT

In what follows, we attempt to establish the linearized DFIG WT model seen from its internal voltage. Perturbing (6), (7) and (10) gives that

$$\Delta E_q = x_m \Delta i_{rd} = \Delta V_q + \frac{x_s}{\omega_{r0}}\Delta i_d - \frac{x_s i_{d0}}{\omega_{r0}^2}\Delta\omega_r \tag{13a}$$

$$\Delta E_d = -x_m \Delta i_{rq} = \Delta V_d - x_s \Delta i_q \tag{13b}$$

$$\Delta\theta_E = (E_{d0}/E_0^2)\Delta E_q - (E_{q0}/E_0^2)\Delta E_d \tag{13c}$$

based on that $\Delta\omega_{slip} = -\Delta\omega_r$. Consider the steady-state, $V_{d0} = V_{d0}^p = V_0 = 1$pu and $V_{q0} = V_{q0}^p = 0$. Linearizing the power equation (11) yields

$$\begin{aligned} \Delta P &= V_{d0}\Delta i_d + i_{d0}\Delta V_d + i_{q0}\Delta V_q, \\ \Delta Q &= -V_{d0}\Delta i_q - i_{q0}\Delta V_d + i_{d0}\Delta V_q \end{aligned} \tag{14}$$

The perturbed terminal voltage and exciting current in the two sets of reference frame related to DFIG WT have the following relationship

$$\begin{aligned} &\Delta V_d^p = \Delta V_d,\ \Delta V_q^p = \Delta V_q - V_{d0}\Delta\theta_p, \\ &\Delta i_{rd}^p = \Delta i_{rd} + i_{rq0}\Delta\theta_p,\ \Delta i_{rq}^p = \Delta i_{rq} - i_{rd0}\Delta\theta_p \end{aligned} \tag{15}$$

Along with the linearization of (12), we have

$$\Delta\theta_p = ((k_{pp}s + k_{ip})/s^2)\Delta V_q^p = G_{pll}(s)\Delta V_q \tag{16}$$

where $G_{pll}(s) = (k_{pp}s + k_{ip})/(s^2 + k_{pp}s + k_{ip})$.

Before moving on, some valid assumptions are made herein: (i) the mechanical power variation ΔP_m is 0 and the mechanical inertia (H) is composed of both the wind turbine and the DFIG; (ii) the rotor speed reference remains unchanged due to the large time constant of MPPT control [11]; (iii) dynamics of the pitch angle and inner current loop are wholly discarded. Thus, the linearized DFIG WT model accounting for (13)-(16) and the control in Fig. 1 can be represented by Fig. 2.

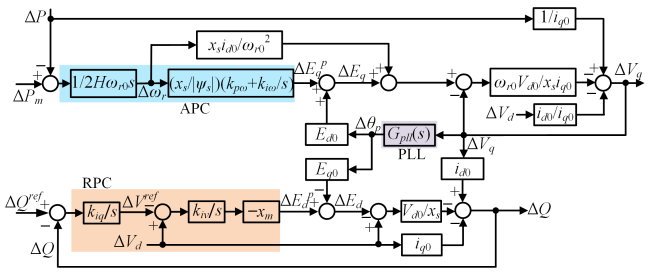

Figure 2. Linearized model of DFIG WT in electromechanical time scale.

Consider that the motion equation of DFIG WT's internal voltage phase is composed of its inertia and damping components. In what follows, we attempt to establish a DFIG WT model seen from the internal voltage motion, and further to extract the inertia and damping components. Recalling (13c), the linearized model in Fig. 2 is hence transformed to Fig. 3, which is constructed seen from the motion of the internal voltage phase and gives a better representation of the electromechanical dynamics for a DFIG WT. In Fig. 3, K_{pv} evaluates the dependency of the terminal voltage on the power perturbation shared by DFIG WT; without loss of generality, $K_{pv} = P_0 V_0 x_g^2/(V_0^4 - (P_0^2 + Q_0^2)x_g^2)$ for a single-WT infinite-bus system (x_g is the grid impedance) will be adopted in the following analysis. It is of interest to note that K_{pv} is non-zero for a grid-connected DFIG WT, while $K_{pv} = 0$ when the inertia of DFIG WT itself is of concern.

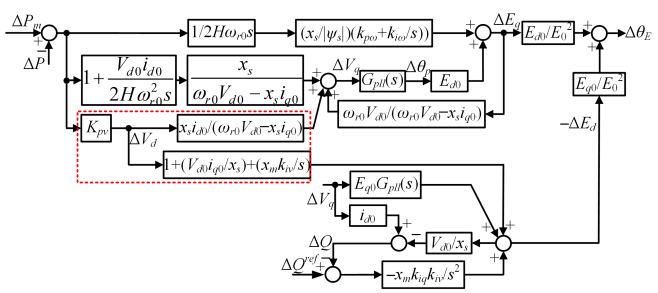

Figure 3. Linearized DFIG WT model seen from the motion of internal voltage phase.

Consider that the reactive power reference (ΔQ^{ref}), given by a secondary control, remains constant [25]. Fig. 3 is accordingly reconstructed to Fig. 4. Therein, M and D are the inertia constant and damping coefficient of the active power control loop, respectively, and

$$M = 2H\omega_{r0}|\psi_s|/(x_s k_{i\omega}),\ D = k_{p\omega}/k_{i\omega} \tag{17}$$

In addition, $m = 2H\omega_{r0}^2/(V_{d0}i_{d0})$, $K_1 = x_s/(\omega_{r0}V_{d0} - x_s i_{q0})$, $K_2 = \omega_{r0}V_{d0}/(\omega_{r0}V_{d0} - x_s i_{q0})$ and $G_{rpc}(s) = (V_{d0}x_m k_{iq}k_{iv}/x_s)/(s^2 + (V_{d0}x_m k_{iq}k_{iv}/x_s))$. K_1 and K_2 vary depending on the reactive loading state (i_{q0}); their polarity would change from positive to negative along with i_{q0} becoming positive and giving that $i_{q0} > \omega_{r0}V_{d0}/x_s$ (i.e., $Q_{e0} < -\omega_{r0}V_{d0}/x_s$ based on (4) and (6)). $G_{pv}(s)$ represents the impacts of the RPC branch on the power angle; it is closely related to the dynamics of PLL (through $G_{pll}(s)$) and RPC (through $G_{rpc}(s)$). It is conceivable that the internal

voltage motion of a DFIG WT is subject to the RPC settings and system loading conditions, aside from the PLL and APC settings.

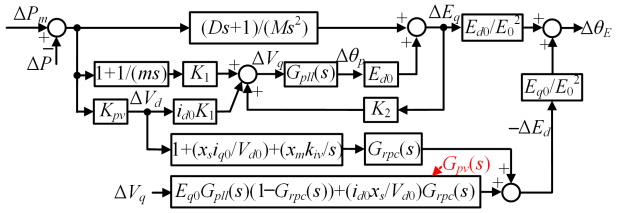

Figure 4. Block diagram of the restructured form of the DFIG WT model.

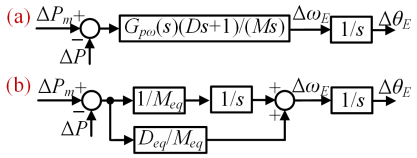

Figure 5. Block diagram of the dynamic between the internal voltage phase and the imbalanced power.

C. Analytic Estimation on DFIG WT's Inertia

The PLL and RPC-related factors are then integrated in the motion equation of the internal voltage phase. An equivalent transformation of Fig. 4 is built and shown in Fig. 5(a) with the following steps. First, ΔV_q is calculated:

$$\Delta V_q = (1/G_1(s))(K_2\frac{Ds+1}{Ms^2} + K_1G_2(s))(\Delta P_m - \Delta P)$$

Second, ΔE_q is calculated:

$$\Delta E_q = (1/G_1(s))(\frac{Ds+1}{Ms^2}+K_1E_{d0}G_{pll}(s)G_2(s))(\Delta P_m-\Delta P)$$

Third, $-\Delta E_d$ is calculated:

$$-\Delta E_d = G_{pv}(s)\Delta V_q+G_{rpc}(s)(1+\frac{x_si_{q0}}{V_{d0}}+\frac{x_mk_{iv}}{s})(\Delta P_m-\Delta P)$$

Forth, $\Delta\theta_E$ is calculated:

$$\Delta\theta_E = (E_{d0}/E_0^2)\Delta E_q + (E_{q0}/E_0^2)(-\Delta E_d)$$

where $G_1(s) = 1-K_2E_{d0}G_{pll}(s)$, $G_2(s) = 1+\frac{1}{ms}+i_{d0}K_{pv}$. The relationship between $\Delta\theta_E$ and $(\Delta P_m - \Delta P)$ can be readily deduced using the four equations above.

In addition, the transfer function $G_{p\omega}(s)$ (see Fig. 5(a)) would change the effect of the inertia M on the internal voltage angle $\Delta\theta_E$ (i.e., the integral of the frequency $\Delta\omega_E$). While $\Delta\theta_E = G_{p\omega}(s)\frac{Ds+1}{Ms^2}(\Delta P_m - \Delta P)$, $G_{p\omega}(s)$ can accordingly be calculated by using the following equation.

$$\begin{aligned} &G_{p\omega}(s)\frac{Ds+1}{Ms^2} = \\ &\frac{1}{G_1(s)}\frac{E_{d0}}{E_0^2}\left[\frac{Ds+1}{Ms^2} + K_1E_{d0}G_{pll}(s)G_2(s)\right] + \\ &\frac{1}{G_1(s)}\frac{E_{q0}}{E_0^2}\left[K_2\frac{Ds+1}{Ms^2} + K_1G_2(s)\right]G_{pv}(s)+ \\ &\frac{E_{q0}}{E_0^2}K_{pv}G_{rpc}(s)(1+\frac{x_si_{q0}}{V_{d0}}+\frac{x_mk_{iv}}{s}) \end{aligned} \tag{18}$$

Fig. 5(b) is obtained by separating the inertia and damping portions, where $M_{eq}(s)$ and $D_{eq}(s)$ are the equivalent inertia and damping coefficient of WT's internal voltage, respectively. The specific swing equation could be written as

$$\frac{D_{eq}(s)s+1}{M_{eq}(s)s^2} = G_{p\omega}(s)\frac{Ds+1}{Ms^2} \tag{19}$$

Before moving on, $G_{pll}(s)$ is rewritten as

$$\begin{aligned} G_{pll}(s) &= \frac{k_{pp}s^2}{(s^2+k_{ip})^2-k_{pp}^2s^2}s + \frac{(k_{ip}-k_{pp}^2)s^2+k_{ip}^2}{(s^2+k_{ip})^2-k_{pp}^2s^2} \\ &= G_{p1}s + G_{p2} \end{aligned}$$

As the displayed in Fig. 5(b), the power imbalance after going through $M_{eq}(s)$ gives an opposite-direction accelerating speed (inspired by [26]). For the sake of convenience, the expression of the reciprocal of $M_{eq}(s)$ is presented here

$$\begin{aligned} \frac{1}{M_{eq}(s)} = &\frac{1}{M_{eq0}} + \frac{1}{M_{eq1}} + \frac{1}{M_{eq2}} + \frac{1}{M_{eq3}} \\ &+ \frac{1}{M_{eq4}} + \frac{1}{M_{eq5}} + \frac{1}{M_{eq6}} + \frac{1}{M_{eq7}} \end{aligned} \tag{20}$$

where

$$\frac{1}{M_{eq0}} = \frac{E_{d0}}{E_0^2}\frac{1}{M} \tag{21a}$$

$$\frac{1}{M_{eq1}} = \frac{E_{d0}}{E_0^2}(\frac{Dk_{pp}}{M} + \frac{k_{ip}}{Ms^2}) \tag{21b}$$

$$\frac{1}{M_{eq2}} = (s^2+k_{ip})\left[\frac{E_{q0}^2}{E_0^2}\frac{K_2}{M}g_1(s) + K_1g_2(s)\right] \tag{21c}$$

$$\frac{1}{M_{eq3}} = k_{pp}\left[\frac{E_{q0}^2}{E_0^2}\frac{K_2}{M}g_3(s) + K_1g_4(s)\right] \tag{21d}$$

$$\frac{1}{M_{eq4}} = -\frac{E_{q0}^2}{E_0^2}G_{rpc}(s)(s^2+k_{ip})\left[\frac{K_2}{M}g_1(s) + K_1g_2(s)\right] \tag{21e}$$

$$\frac{1}{M_{eq5}} = -\frac{E_{q0}^2}{E_0^2}G_{rpc}(s)k_{pp}\left[\frac{K_2}{M}g_3(s) + K_1g_4(s)\right] \tag{21f}$$

$$\frac{1}{M_{eq6}} = \frac{E_{q0}}{E_0^2}G_{rpc}(s)\frac{x_si_{d0}}{V_{d0}}\left[(s^2+k_{ip})g_5(s) + k_{pp}g_6\right] \tag{21g}$$

$$\frac{1}{M_{eq7}} = \frac{E_{q0}}{E_0^2}G_{rpc}(s)K_{pv}(1+\frac{x_si_{q0}}{V_{d0}})s^2 \tag{21h}$$

associated to the notations that $g_1(s) = DG_{p1} + G_{p2}/s^2$, $g_2(s) = G_{p1}/m+(1+i_{d0}K_{pv})G_{p2}$, $g_3(s) = DG_{p2}+G_{p1}/s^2$, $g_4(s) = G_{p2}/m+(1+i_{d0}K_{pv})G_{p1}s^2$, $g_5(s) = K_2/(Ms^2)+K_1(1+i_{d0}K_{pv})$, and $g_6 = DK_2/M + K_1/m$.

Observations from (20) and (21) give the following. (i) The first term M_{eq0} is the APC inertia. (ii) M_{eq1}, M_{eq2} and M_{eq3} are caused by PLL, representing the participation of PLL in the inertia provision of DFIG WT. The implication of (i) and (ii) is that the parallel APC and PLL constitute part of the inertia $M_{eq}(s)$. (iii) M_{eq4} to M_{eq7} are caused by RPC and PLL, and they are all zero by assumption of no RPC impacts considered. In addition, M_{eq2} to M_{eq6} would vary with the system loading condition due to the involved K_1 and K_2. Therefore, the formulation of $M_{eq}(s)$ in (20) and (21) offers

an analytical and mathematical way to examine the impacts of PLL (k_{pp}, k_{ip}), RPC (k_{iq}, k_{iv}) and K_1, K_2 (varying with the reactive loading state) on the inertia $M_{eq}(s)$.

D. Discussion

Based on (20), we get that the value of $1/M_{eq}(s)$ is much more sensitive to $1/M_{eqi}(i = 0, 1, \dots \text{ or } 7)$ with a larger value. That is, a smaller $M_{eqi}(i = 0, 1, \dots \text{ or } 7)$ plays a more important role in determining the value of $M_{eq}(s)$. Some important findings can then be obtained under a specific loading condition.

- The items $1/M_{eqi}(i = 4, 5, 6 \text{ or } 7)$ can be discarded in (20) by considering that $|G_{rpc}(s)| \ll 1$ in the conceivable frequencies and hence that $1/M_{eqi}(i = 4, 5, 6 \text{ or } 7) \ll 1/M_{eqi}(i = 1, 2, \text{ or } 3)$ in accordance to (21).
- For a fast-action PLL, $1/M_{eqi}(i = 1, 2, \text{ or } 3)$ are relatively large and $1/M_{eq0}$ can also be discarded in (20). Thus, $1/M_{eq}(s)$ is accordingly determined by the three items $1/M_{eqi}(i = 1, 2, \text{ or } 3)$.
- For a slow-action PLL, $1/M_{eq0}$ becomes nontrivial with respect to $1/M_{eqi}(i = 1, 2, \text{ or } 3)$. Thus, $1/M_{eqi}(i = 0, 1, 2, \text{ or } 3)$ should be all included when evaluating the overall inertia $M_{eq}(s)$.
- In the case of a slow-action PLL, $M_{eqi}(i = 4, 5, 6 \text{ and } 7)$ become non-negligible, but their influences on the inertia $M_{eq}(s)$ are still relatively small compared to $M_{eqi}(i = 0, 1, 2 \text{ and } 3)$. However, they should also be included in (20) when evaluating the influence of RPC settings on the inertia $M_{eq}(s)$.

Therefore, the PLL behavior imposes a nontrivial impact on the inertia $M_{eq}(s)$ and a considerable inertia could be obtained by tuning the PLL settings. The property of $M_{eq}(s)$ is also impacted by the RPC settings and operating conditions. These will be examined in details in the next section.

IV. Impacts of PLL and RPC on the Inertia Provision by DFIG WT

In this section, (20) and (21) are employed to analytically evaluate the impacts of PLL and RPC-related factors on inertia provision by DFIG WT. In this analysis, the character study on the equivalent inertia $M_{eq}(s)$ is carried out by considering different PLL and RPC parameter settings, and a wide range of reactive loading state from a reactive injection to a reactive absorption state.

A. Impact of PLL on the Inertia $M_{eq}(s)$

1) Character study on $M_{eq}(s)$ under different PLL settings: In this segment, the character of the inertia of DFIG WT itself is of concern, which is determined by the control parameters and the operating state of WT itself, but independent from the grid condition. $M_{eq}(s)$ is accordingly obtained from (20) and (21), along with letting $K_{pv} = 0$. A further investigation on (20) and (21) promises that the value of $M_{eq}(s)$ is negatively correlated with (k_{pp}, k_{ip}) of PLL. In what follows, we consider five pairs of (k_{pp}, k_{ip}), which make the PLL bandwidth change from 13.3 Hz to 0.133 Hz while keeping the PLL damping ratio constant ($= 0.8$). Consider the case of synchronous speed operation ($\omega_{r0} = 1$ p.u.), it admits that the polarity of K_1 and K_2 changes from positive to negative around at $Q_0 = -\omega_{r0} V_{d0}/x_s = -0.33$ p.u. (refer to the DFIG WT parameters in Appendix. B). Meanwhile, (k_{iq}, k_{iv}) of RPC are kept at $(0.05, 20)$ [22]. The value of $M_{eq}(s)$ under these cases are illustrated in Fig. 6.

Fig. 6 shows that (i) at a given reactive loading state, $M_{eq}(s)$ increases with the decrease of (k_{pp}, k_{ip}). However $M_{eq}(s)$ approaches to 0 at $Q_0 = -0.3$ p.u. and becomes negative under deep reactive absorption states ($Q_0 < -0.33$ p.u., like $Q_0 = -0.4$ p.u. and $Q_0 = -0.5$ p.u.); (ii) $M_{eq}(s)$ has a relatively large value under the case of a high reactive injection. Thus, tuning PLL parameters is an alternative way to achieve the inertia provision by DFIG WT. This method is simple and cost-effective for inertia emulation in practice, but the drawback is the risk of the negative inertia under deep reactive absorption states.

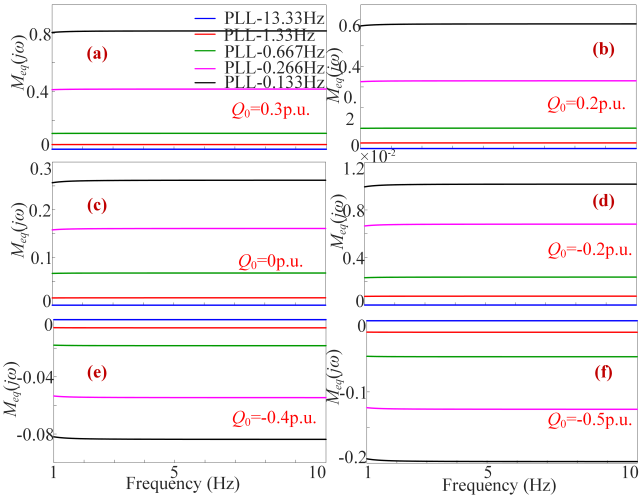

Figure 6. The value of $M_{eq}(s)$ with respect to (k_{pp}, k_{ip}) of PLL under a reactive loading state from the reactive injection ($Q_0 = 0.3$ p.u.) to the reactive absorption ($Q_0 = -0.5$ p.u.).

2) Analytical description on the effect of a slow-action PLL: An analytical explanation on the effect of slowing PLL is presented in Appendix. B. In the case of $i_{q0} < \omega_{r0} V_{d0}/x_s$, the equivalent power angle δ_p lies in $(0, \pi/2)$ and the increase of the power angle would produces an over-production power output. A positive inertia provision is accordingly produced. In contrast, under $i_{q0} > \omega_{r0} V_{d0}/x_s$, the equivalent power angle δ_p lies in $(\pi/2, \pi)$ and the increase of the power angle might produce an under-production power output. It hence implies a negative inertia provision.

3) Improved inertia emulation through PLL: To circumvent the negative inertia phenomena, PLL should be performed with fast-tracking function, rather than the inertia emulation. In this case, an alternative inertia emulation method can be implemented by fabricating a negative feedback of the signal V_q^p to superpose on the rotor-side torque reference (see Fig. 7). Discarding the PLL output error yields

$$\Delta V_q = \Delta\theta_p = \frac{k_{pp}s + k_{ip}}{s^2}\Delta V_q^p \approx \frac{1}{s^2} k_{ip} \Delta V_q^p \qquad (22)$$

by the assumption $k_{pp} << kip$ [23], [28]. The supplemented feedback control is deployed with $k_{ip}\Delta V_q^p$ as the input and k_{vt} as the control gain.

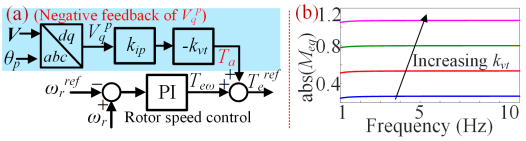

Figure 7. V_q^p feedback control for inertia emulation.

Following a similar derivation in Section III (while a fast-action PLL is applied here), the obtained equivalent inertia can be written as

$$\begin{aligned}\frac{1}{M_{eq}(s)} &= \frac{E_{d0}}{E_0^2}\frac{1}{1+x_s k_{vt} K_2 s^2}\left(\frac{1}{M}+\frac{K_1}{K_2}s^2\right) \\ &\approx \frac{E_{d0}^2}{E_0^2}\frac{1}{\omega_{r0}^2 V_{d0}^2 k_{vt}}\end{aligned} \tag{23}$$

where the "≈" is established by the assumption $k_{vt} >> 1$ and $(K_1/K_2) = (x_s/\omega_{r0}V_{d0}) >> (1/M)$ (refer to [22], $K_1/K_2 \approx 3.08$ and $1/M \approx 0.18$). For one thing, the equivalent inertia $M_{eq}(s)$ (in (23)) of the V_q^p feedback control keeps positive and proportional to the gain k_{vt}. For another thing, (22) declares that $k_{ip}\Delta V_q^p$ is equivalent to the frequency derivative when $(k_{pp} << k_{ip})$. That is, the developed V_q^p feedback control is inherently equivalent to the commonly used df/dt inertia control [22]. However, it is preferable due to the avoidance of a pure derivative term.

B. Impact of RPC on the Inertia $M_{eq}(s)$

1) Character study on $M_{eq}(s)$ under different RPC settings: The scenario of a grid-connected DFIG WT is considered to examine the impacts of RPC on the inertia $M_{eq}(s)$. $M_{eq}(s)$ is then calculated following a non-zero K_{pv} (obtained when $x_g = 1.26$ p.u.) and different RPC parameters (k_{iq}, k_{iv}) in (20) and (21). While keeping (k_{pp}, k_{ip}) of PLL set at $(3, 3.5)$ for inertia emulation, the RPC bandwidth decreases with changing the parameters (k_{iq}, k_{iv}) from $(0.05, 20)$ to $(0.005, 0.2)$. Fig. 8 displays the resulted value of $M_{eq}(s)$ under three reactive loading states.

Fig. 8 shows the following. (i) Compared to the case of $K_{pv} = 0$, $M_{eq}(s)$ has a relatively small value for the case of a non-zero K_{pv}. This is because that K_{pv} is usually positive since a power vacancy in the system would create a negative voltage deviation, thereby restraining the over-production power from DFIG WT. (ii) The value of a positive $M_{eq}(s)$ decreases with the reduce of (k_{iq}, k_{iv}), while the absolute value of a negative $M_{eq}(s)$ increases with the reduce of (k_{iq}, k_{iv}). Thus, a pair of small (k_{iq}, k_{iv}) leads to a prolonged voltage excursion, which further deteriorates the inertia provision of DFIG WT.

2) Analytical description on the effect of RPC: The effect of RPC on the inertia provision is briefly described as follows. When the tied system suffers an abrupt load pick-up, a phase lag and a magnitude drop of node voltages maybe simultaneously occur [27]. Then the system attempts to restore its node voltages, still lacking the reactive power supply. Meanwhile, RPC still tries to track its reactive reference by absorbing more reactive power from the system. These would provoke a continuous shortage of reactive power and a failing voltage resumption, and further a constraint on the availability of over-production power delivery. A desired inertia provision is accordingly difficult to achieve, especially in the case of a degraded voltage regulation by a slow-action RPC. To preserve a positive inertia, it is advisable to ensure a fast-responding RPC and a sustainable local var compensation.

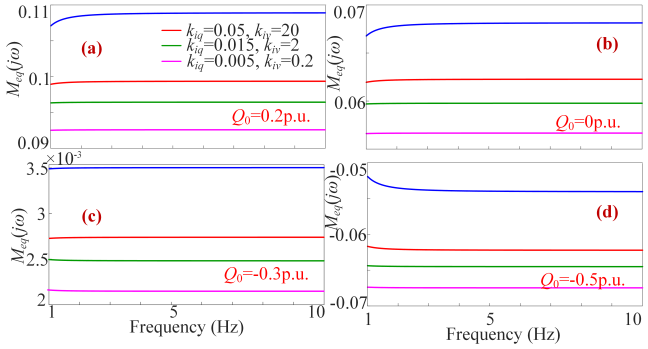

Figure 8. The value of $M_{eq}(s)$ with respect to (k_{iq}, k_{iv}) of RPC under $Q_0 = 0.2$, 0, -0.3 and -0.5 p.u. (Note: the blue line is obtained under $K_{pv} = 0$.

*3) **Remark**:* The inertia provision would be degraded in case of RPC used, due to a possible continuous shortage of the system reactive power. This phenomenon is conceived to be more serious in a reactive-absorption mode of DFIG WTs. As shown in Fig. 8, the equivalent inertia $M_{eq}(s)$ decreases with the reactive power loading level deceasing from 0.2 p.u. to -0.5 p.u. $M_{eq}(s)$ finally becomes negative when DFIG WTs operate with a 0.5-p.u. reactive power absorption (i.e., $Q_0 = -0.5$ p.u.).

V. Simulation Study

The simulation studies are conducted in a typical three machine-nine node system in MATLAB/SIMULINK. The system topology is shown in Fig. 9. G1 is a 247.5 MW hydro turbine generator and G2 is a 192 MW gas turbine generator. They are equipped with droop and excitation control systems [24]. G3 is an aggregated DFIG WTs with rated power at 180 MW (i.e., $120 * 1.5$ MW). The aerodynamic system, pitch control, converter system and electrical control are all included in the WT model (referred to the wind farm testbed in [28]). Other parameters of the test system are listed in Appendix. C.

In the simulation, the wind speed is kept at 9.32 m/s and the instantaneous penetration of wind power reaches 23.22% under the normal operation. The PLL and RPC parameters are initially set as $(k_{pp},\ k_{ip}) = (3,\ 3.5)$ (for inertia emulation), and $(k_{iq},\ k_{iv}) = (0.05,\ 20)$. The analysis results will be validated by the following simulations.

1) Evaluate the impact of PLL on the inertia emulation by DFIG WT;
2) Evaluate the impact of RPC on the inertia emulation by DFIG WT;

3) Demonstrate the effectiveness of the V_q^p feedback control in mitigating the negative-inertia impact.

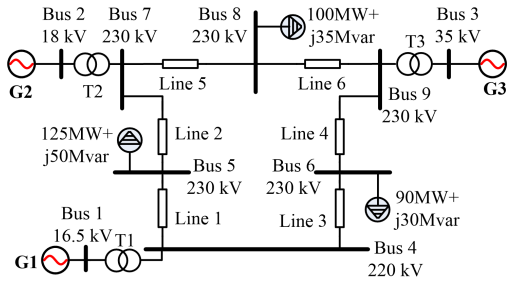

Figure 9. Three machine-nine nodes test system.

A. Impact of PLL on Inertia Provision

First, the inertia character of DFIG WT depending on PLL is examined against two scenarios where DFIG WT operates in a (i) reactive injection state ($Q_0 = 0$) or (ii) a reactive absorption state ($Q_0 = -0.4$ p.u.). A low-frequency event is created by a step load increment (20 MW) at bus 6 at $t = 1$ s.

Fig. 10 depicts the consequent inertial responses of DFIG WT. The observations show that (i) under $Q_0 = 0$, DFIG WT has a positive inertia emulation through a slow-action PLL, and such an inertia is larger for a reduced PLL bandwidth; (ii) under $Q_0 = -0.4$ p.u., the emulated inertia of DFIG WT becomes negative, and it has a larger magnitude for a reduced PLL bandwidth (notably, the system loses its stability with further decreasing the PLL bandwidth to 0.266 Hz).

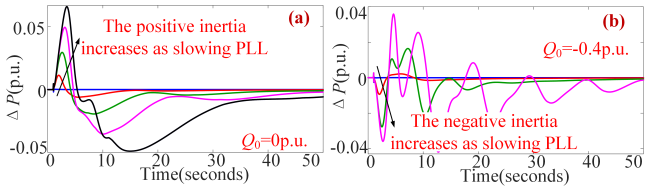

Figure 10. Responses under different PLL settings: (a) $Q_0 = 0$ p.u.; (b) $Q_0 = -0.4$ p.u. (Note: blue line-PLL with 13.33 Hz; red line-PLL with 1.333 Hz; green line-PLL with 0.667 Hz; purple line-PLL with 0.443 Hz; black line-PLL with 0.266 Hz).

In addition, the PLL bandwidth is kept at 1.33 Hz and a wide range of reactive loading conditions is simulated ($Q_0 = 0.4 \sim -0.5$ p.u.). G3 increases to 300 MW to have a large participation in system frequency dynamics. A same low-frequency event occurs and G3 has an inertial response as shown in Fig. 11.

Observations from Fig. 11 give some important findings. (i) The inertia emulated by DFIG WT increases with the reactive loading state changing from $Q_0 = -0.2$ p.u. to $Q_0 = 0.4$ p.u. (see Fig. 11 (a)). (ii) Once DFIG WT operates at $Q_0 < -0.31$ p.u. (i.e., the absorbed reactive power larger than 0.31 p.u.), a condition where the inertia goes from positive to negative is created. (iii) The negative inertia increases with the level of reactive absorption, as depicted by Fig. 11 (c). (iv) The negative inertia would incur a deteriorated system frequency performance (see Fig. 11 (d)).

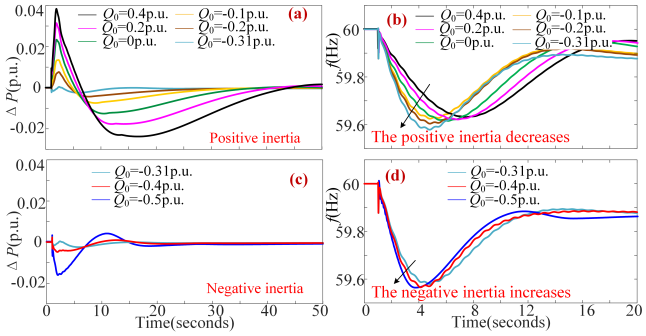

Figure 11. Responses under different reactive loading states: (a), (c) Upward active power output (p.u.); (b), (d) System frequency (Hz).

B. Impact of RPC on Inertia Provision

In this segment, the impact of RPC on the inertia provision by DFIG WT is evaluated. This is conducted against two scenarios where DFIG WT operates with (i) a positive inertia emulation ($Q_0 = 0$) or (ii) a negative inertia emulation ($Q_0 = -0.5$ p.u.). At $t = 1$ s, the test system has a a step load increment (20 MW) at bus 6.

Fig. 12 illustrates the simulation results. (i) Fig. 12 (a)-(b) are obtained under $Q_0 = 0$ and they show that the inertial response of DFIG WT reduces as the RPC becomes slower. This is because that slowing RPC leads to a prolonged voltage transient (see Fig. 13), hence restraining the over-production power delivery from DFIG WT. Beyond this point, Fig. 12 (c)-(d) depict the responses of DFIG WT under $Q_0 = -0.5$ p.u. and a negative inertia is created in this case. It can be seen that the adverse impact of negative inertia would be exacerbated with the decrease of RPC speed. In addition, Fig. 12 promises that under the case of a slower-action PLL, a larger impact of the RPC speed on the inertia provision by DFIG WT would be incurred.

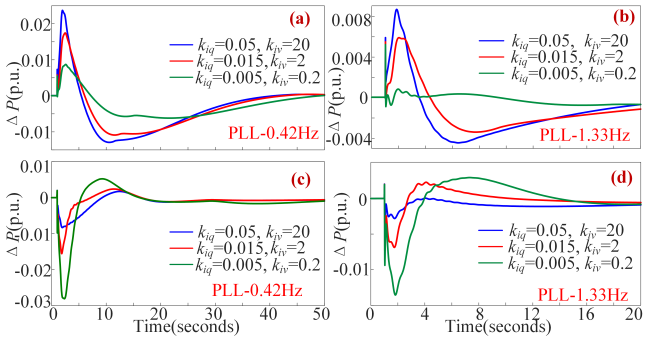

Figure 12. Responses under different RPC speeds and PLL bandwidths ((a)-(b): $Q_0 = 0$; (c)-(d): $Q_0 = -0.5$ p.u.)

C. V_q^p Feedback Control for Improving Inertia Emulation

In this segment, a simulation scenario where a negative inertia is emulated by DFIG WT is considered. Specifically, (k_{iq}, k_{iv}) are set as $(0.015, 2)$ and $Q_0 = -0.5$ p.u. To circumvent the phenomenon of a negative inertia emulation, a V_q^p feedback control is proposed to realize the inertia emulation of DFIG WT. Notably, regardless of control cost

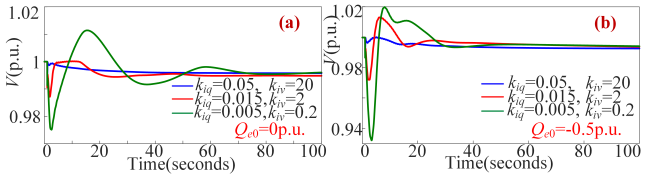

Figure 13. Terminal voltage transients under different RPC speeds.

or inconvenience, df/dt inertia control (using a washout filter supplement to mimic the derivative term) and virtual synchronous control (VSynC, in [13]) might be both alternative for inertia emulation. The effectiveness of these controls is demonstrated in Fig. 14. Therein, the gain for V_q^p feedback control is set as 50; the gain and filter time constant for df/dt inertia control are set as 10 and 5.5 [22], respectively; the virtual inertia and damping coefficients for VSynC are set as 10 and 60, respectively.

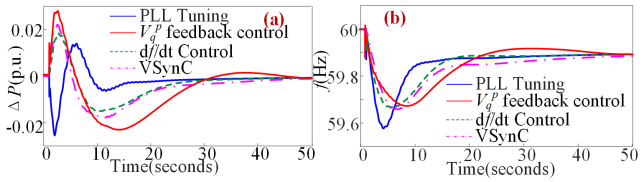

Figure 14. Responses under different inertia control strategies: (a) Upward active power output (p.u.); (b) System frequency (Hz).

VI. Conclusion

This paper evaluated the impacts of PLL and RPC on the inertia provision by DFIG WT. A linearized DFIG WT model, seen from the internal voltage phase motion, was established to facilitate the analytical estimation on WTs' equivalent inertia. The impacts of PLL and RPC were examined through measuring the equivalent inertia and detecting the inertia character under different PLL and RPC settings. The analytical study demonstrated that (i) slowing PLL (i.e., decreasing the PLL bandwidth) is an alternative way for DFIG WT to realize inertia provision and the inertia provision can be further enhanced with the increase of the reactive-injection level; (ii) the inertia provision would be decreased when small (k_{iq}, k_{iv}) of RPC engage; (iii) although the inertia provision by DFIG WT may be positive under most system loading conditions, it may become negative under the deep reactive-absorption condition; (iv) the negative inertia phenomena can be circumvented by the proposed V_q^p feedback control that is conceived to be a preferable way for DFIG WT's inertia emulation, since it is cost-effective and can be simply implemented. All of them were verified by simulation tests.

To summarize, the linearized model in the analysis provides a better understanding and a good estimation on DFIG WT's inertia provision; the analysis results allow to observe an identification on the inertia character of a DFIG WT under possible control settings and system loading conditions. This would be useful for the manufacturers to guide/improve their inertia control design and for the operators to evaluate/correct the possible negative inertia phenomenon in power systems.

Appendix

A. Two Frames Associated with DFIG WT

In this context, there are two sets of reference frame related to DFIG WT used. The conversion matrixes between them are

$$T_{t\to p} = \begin{bmatrix} \cos\theta_p & -\sin\theta_p \\ \sin\theta_p & \cos\theta_p \end{bmatrix}$$
$$T_{p\to t} = \begin{bmatrix} \cos\theta_p & \sin\theta_p \\ -\sin\theta_p & \cos\theta_p \end{bmatrix} \quad (24)$$

B. Analytical description on the effect of a slow-action PLL

To facilitate the following analysis, a fictitious internal voltage $\boldsymbol{E_p}$ is defined

$$\boldsymbol{E_p} = E_{pd} + jE_{pq} = (E_d - (1-\omega_r)V_d) + j\omega_r E_q \quad (25)$$

When combining (10) and (11), the active power equation of DFIG WT could be written as

$$P = -(\omega_r V_d/x_s)(V_q - E_q) + (V_q/x_s)(V_d - E_d) \quad (26)$$

By invoking (25), (26) becomes

$$P = (1/x_s)(-E_{pd}V_q + E_{pq}V_d) = (E_p V/x_s)\sin\delta_p \quad (27)$$

where δ_p is the phase angle separating between the vectors $\boldsymbol{E_p}$ and $\boldsymbol{V}$ (see the phasor diagram depicted by Fig. 15). Therein, $\boldsymbol{V'}$ is the post-disturbance terminal voltage vector and δ'_p is the post-disturbance angle between $\boldsymbol{E'_p}$ and $\boldsymbol{V'}$; d_{PLL} and d'_{PLL} are the d axis of the PLL frame under the pre- and post- disturbance case. For the sake of analysis, we assume that (i) the PLL is extremely slow and its position does not move after the disturbance; (ii) the fictitious internal voltage vector $\boldsymbol{E_p}$ controlled in the PLL frame does not change either. Fig. 15 (a) and (b) show the relationship between $\boldsymbol{E_p}(/\boldsymbol{E'_p})$ and $\boldsymbol{V}(/\boldsymbol{V'})$ under $E_{pd} > 0$ (or δ_p within $(0, \pi/2)$) and $E_{pd} < 0$ (δ_p within $(\pi/2, \pi)$), respectively. It is of interest to note that the operating characteristics of DFIG WT shown in Fig. 15 (a) and (b) is similar to the lagging and leading power factor operation of SGs [24].

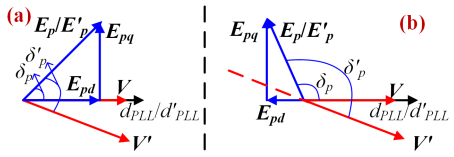

Figure 15. Phasor diagram of the vectors $\boldsymbol{E_p}(/\boldsymbol{E'_p})$ and $\boldsymbol{V}(/\boldsymbol{V'})$: (a) $E_{pd} > 0$, (b) $E_{pd} < 0$.

Following the equations (4)-(6), (28) can be obtained and expressed as

$$E_{pd} = (1-\omega_r)V_d - E_d = \omega_r V_d - x_s i_q \quad (28)$$

Consider a step increment of load power event which makes δ_p change to δ'_p. (i) If $E_{pd} > 0$ under $i_q < \omega_r V_d/x_s$, the output power P would increase (in accordance to (27)) when δ_p changes to δ'_p after the event. It means that a positive inertia provision is created to compensate the power vacancy. (ii) If $E_{pd} < 0$ under $i_q > \omega_r V_d/x_s$, the output power P would decrease (in accordance to (27)) when δ_p changes to δ'_p after

the event. It means that a negative inertia provision is created to make the power vacancy deteriorated. When considering the movement of a slow-action PLL (d'_{PLL} is slightly lagged behind d_{PLL}), δ'_p would be slightly smaller than the value under a d'_{PLL}-invariant case. It implies that the amount of the over-production power (for a positive inertia) and the under-production power (for a negative inertia) would be also slightly smaller while the findings in (i) and (ii) still hold.

C. Simulation Test System Parameters

G1 parameters (on Base of Machine Rating)

$P_n = 247.5MW, V_n = 16.5kV, X_d = 0.36, X'_d = 0.15,$ $X''_d = 0.1, X_q = 0.24, X''_q = 0.2, R_a = 0.003, X_l = 0.083, T'_{d0} = 8.96, T_d0'' = 0.05, T''_{q0} = 0.03, H = 9.55s$, pole pairs 20. Hydraulic unit and governor parameters: $K_g = 20, T_G = 0.2s, T_W = 0.3s, T_R = 5s, R_T = 0.38.$

G2 parameters (on Base of Machine Rating)

$P_n = 192MW, V_n = 18kV, X_d = 1.72, X'_d = 0.23, X''_d = 0.2, X_q = 1.66, X'_q = 0.378, X''_q = 0.30, R_a = 0.003, X_l = 0.15, T'_{d0} = 6, T_d0'' = 0.03, T'_{q0} = 0.535, T''_{q0} = 0.07, H = 3.33s$, pole pairs 20. Steam turbine and governor parameters: $K_g = 20, T_G = 0.2s, T_{CH} = 0.3s, T_{RH} = 7s, F_{HP} = 0.3.$

DFIG WT Parameters (on Base of Machine Rating)

$P_n = 1.5MW, V_n = 690V, \omega_b = 120\pi, R_s = 0.023, R_r = 0.016, L_s = 3.08, L_r = 3.06, L_m = 2.9$, Speed control:$k_{p\omega} = 3, k_{i\omega} = 0.6$, Pitch angle control: $k_{pp} = 3, k_{ip} = 30$, Current control(RSC): $k_{pir} = 0.6, k_{iir} = 8$, Reactive power control (RSC): $k_{iq} = 0.05, k_{iv} = 20$, Filter resistance: $R_f = 0.003$p.u., $L_f = 0.3$p.u., DC capacitor: $C = 10000\mu F$, DC voltage: $U_{dc} = 1150V$, DC voltage control (GSC):$k_{pdc} = 8, k_{idc} = 400$, Current control (GSC):$k_{pig} = 0.83, k_{iig} = 5$, PLL parameters: $k_{pp} = 60, k_{ip} = 1400.$

REFERENCES

[1] D. G. Photovoltaics, and E. Storage, "IEEE standard for interconnection and interoperability of distributed energy resources with associated electric power systems interfaces," *IEEE Std*, 1547-2018, Apr. 2018.

[2] M. H. Bollen, and F. Hassan, *Integration of distributed generation in power system*, 1^{st} edition, USA, NJ, Hoboken: Wiley, 2011.

[3] National Code, "The Grid Code (Issue 5)," Mar. 2017. [Online]. Available: https://www.nationalgrid.com/sites/default/files/documents/8589935310-Complete%20Grid%20Code.pdf

[4] Hydro-Qubec Transnergie, "Transmission provider technical requirements for the connection of power plants to the Hydro-Qubec transmission system," Quebec, Tech. Rep. Feb. 2009.

[5] P. L. Denholm, Y. Sun, and T. T. Mai, "An introduction to grid services: Concepts, technical requirements, and provision from wind," National Renewable Energy Lab. (NREL), Golden, CO (United States), Tech. Rep., 2019.

[6] N. Pahalawaththa, S. Achilles, K. Elkington, et al, "Connection of wind farms to weak AC networks," Working Group B4.62, Cigre, Tech. Rep., Dec. 2016.

[7] V. Gevorgian, Y. Zhang, and E. Ela, "Investigating the impacts of wind generation participation in interconnection frequency response," *IEEE Trans. Sustainable Energy*, vol. 6, no. 3, pp. 1004-1012, July 2015.

[8] J. Morren, S. W. H. de Haan, W. L. Kling, and J. A. Ferreira, "Wind turbines emulating inertia and supporting primary frequency control," *IEEE Trans. Power Syst.*, vol. 21, no. 1, pp. 433-434, Feb. 2006.

[9] A. B. Attya, J. L. Dominguez-Garcia, and O. Anaya-Lara, "A review on frequency support provision by wind power plants: Current and future challenges," *Renewable and Sustainable Energy Reviews*, vol. 81, no. 2, pp. 2071-2087, Jan. 2018.

[10] M. F. M. Arani, and E. F. El-Saadany, "Implementing virtual inertia in DFIG-based wind power generation," *IEEE Trans. Power Syst.*, vol. 28, no. 2, pp. 1373-1384, May 2013.

[11] W. He, X. Yuan, and J. Hu, "Inertia provision and estimation of PLL-based DFIG wind turbines," *IEEE Trans. Power Syst.*, vol. 32, no. 1, pp. 510-521, Jan. 2017.

[12] X. Zhu, Y. Wang, L. Xu, X. Zhang, and H. Li, "Virtual inertia control of DFIG-based wind turbines for dynamic grid frequency support," in *IET Conference on Renewable Power Generation (RPG)*, Edinburgh, UK, pp. 224-224, Sept. 2011.

[13] S. Wang, J. Hu, X. Yuan, and L. Sun, "On inertial dynamics of virtual-synchronous-controlled DFIG-based wind turbines," *IEEE Trans. Energy Convers.*, vol. 30, no. 4, pp. 1691-1702, Dec. 2015.

[14] S. Engelhardt, I. Erlich, C. Feltes, J. Kretschmann, and F. Shewarega, "Reactive power capability of wind turbines based on doubly fed induction generators," *IEEE Trans. Energy Convers.*, vol. 26, no. 1, pp. 364-372, Mar. 2011.

[15] A. Moeini, and I. Kamwa, "Analytical concepts for reactive power based primary frequency control in power systems," *IEEE Trans. Power Syst.*, vol. 31, no. 6, pp. 4217-4230, Nov. 2016.

[16] J. Hu, Y. Huang, D. Wang, H. Yuan, and X. Yuan, "Modeling of grid-connected DFIG-based wind turbines for DC-link voltage stability analysis," *IEEE Trans. Sustain. Energy*, vol. 6, no. 4, pp. 1325-1336, Oct. 2015.

[17] Y. Zhang and B. T. Ooi, "Stand-alone doubly-fed induction generators (DFIGs) with autonomous frequency control," *IEEE Trans. Power Delivery*, vol. 28, no. 2, pp. 752-760, Apr. 2013.

[18] N. W. Miller, K. Clark, and M. Shao, "Frequency responsive wind plant controls: Impacts on grid performance," In *Power and Energy Society General Meeting, 2011 IEEE*, San Diego, CA, USA, July 2011.

[19] G. C. Tarnowski, "Coordinated frequency control of wind turbines in power systems with high wind power penetration," *PhD thesis*, Technical University of Denmark, Lyngby, 2011.

[20] L. Ruttledge, N.W. Miller, J. O'Sullivan and D. Flynn, "Frequency response of power systems with variable speed wind turbines," *IEEE Transactions on Sustainable Energy.*, vol. 3, no. 4, pp. 683-691, Oct. 2012.

[21] ENTSO-E, "ENTSO-E draft requirements for grid connection applicable to all generators," 2011.

[22] K. Clark, N. W. Miller, and J. J. Sanchez-Gasca, "Modeling of GE wind turbine-generators for grid studies," GE Inc., Schenectady, NY, Tech. Rep. Version 4.5, Apr. 2010.

[23] J. Hu, H. Xu, and Y. He, "Coordinated control of DFIG' s RSC and GSC under generalized unbalanced and distorted grid voltage conditions," *IEEE Trans. Ind. Electron.*, vol. 60, no. 7, pp. 2808-2819, July 2013.

[24] P. Kundur, *Power system stability and control*, New York: McGraw-Hill, 1994.

[25] Y. Guo, S. H. Hosseini, C. Y. Tang, J. N. Jiang, and R. G. Ramakumar, "An approximate wind turbine control system model for wind farm power control," *IEEE Trans. Sustain. Energy*, vol. 4, no. 1, pp. 262-274, Jan. 2013.

[26] H. Yuan, X. Yuan, and J. Hu, "Modeling of grid-connected VSCs for power system small-signal stability analysis in DC-link voltage control timescale," *IEEE Trans. Power Syst.*, vol. 32, no. 5, pp. 3981-3991, Sept. 2017.

[27] J. J. Grainger, and W. D. Stevenson, *Power system analysis*, New York: McGraw-Hill, 1994.

[28] The MathWorks, "Wind Farm-DFIG Average Model," Mar. 2012 (accessed Nov. 2013). [Online]. Available: https://mathworks.com

Li Sun received the B. Eng. degree and the M.Eng. degrees from Huazhong University of Science and Technology (HUST), Wuhan, China, in 2013, and 2016 respectively, and the Ph.D. degree from The University of Hong Kong, Hong Kong, in 2019, both in electrical engineering. She is currently a Research Fellow with the University of Warwick, United Kingdom. Her current research interests focus on the power system stability control, control design and optimization of islanded microgrids.

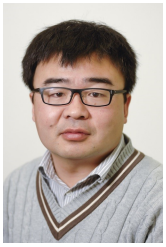

Xiaowei Zhao is Professor of Control Engineering and an EPSRC Fellow at the School of Engineering, University of Warwick, Coventry, UK. He obtained the PhD degree in Control Theory from Imperial College London in 2010. After that he worked as a postdoctoral researcher at the University of Oxford for three years before joining Warwick in 2013. His main research areas are control theory with applications on offshore renewable energy systems, local smart energy systems, and autonomous systems.